Operational Stability Limits in Rotating Detonation Engine Numerical Simulations

Daniel E. Paxson*
NASA Glenn Research Center, Cleveland, Ohio, 44130

Douglas A. Schwer†
Naval Research Laboratory, Washington, District of Columbia 20375

An instability is described which arises in computational fluid dynamic (CFD) simulations of semi-idealized rotating detonation engines (RDE) configured with a throat at the exit. Its existence is verified by examining output from two independently developed CFD codes simulating the same configuration and producing solutions that agree well. The instability is shown to be thermo-acoustic in that a spatial integral of the product of pressure and heat release fluctuations develops a regular oscillation which grows in time. The instability can become severe enough to cause detonation failure. Its onset is shown to be closely linked to the size of the exit throat and the size of the inlet restriction; both parameters that strongly influence RDE performance. It is shown that the instability places a cap on ideal RDE performance, but that an optimized exhaust throat and inlet restriction combination still yields substantial pressure gain. Other parametric sensitivities are also examined in terms of instability growth. These include axial length, inlet manifold pressure, and air-fuel ratio.

Nomenclature

A_{ch}	=	channel (annulus) cross sectional area
A_{th}	=	exit throat cross sectional area
A_i	=	inlet restriction cross sectional area
a^*	=	reference speed of sound
EAP_i	=	Equivalent Available Pressure (ideal)
ER	=	Equivalence Ratio
h_f	=	fuel heating value
L	=	circumference
l	=	axial length
N	=	maximum grid point index
P_m	=	manifold pressure
P_a	=	ambient pressure
p	=	non-dimensional pressure
p^*	=	reference pressure
p'	=	non-dimensional pressure fluctuation
q	=	non-dimensional heat release rate
q'	=	non-dimensional heat release rate fluctuation
R_g	=	real gas constant
R_c	=	Rayleigh integral
T	=	non-dimensional temperature
T_m	=	manifold temperature
T^*	=	reference temperature
t	=	non-dimensional time
t_{rev}	=	non-dimensional time for one detonation revolution

*Aerospace Research Engineer, Research and Engineering Directorate, 21000 Brookpark Road/MS 77-1, AIAA Associate Fellow
† Mechanical Engineer, Laboratories for Computational Physics and Fluid Dynamics. Senior Member AIAA

u = non-dimensional circumferential velocity
u_{det} = non-dimensional detonation velocity
v = non-dimensional axial velocity
x = non-dimensional circumferential dimension
Y' = fluctuating quantity to be summed
y = non-dimensional axial dimension
z = non-dimensional radial dimension

Greek
Δ = numerical spatial difference
γ = ratio of specific heats
φ = generic quantity
$\overline{\varphi}$ = mass flux-averaged generic quantity
ρ = non-dimensional density
ρ^* = reference density

Subscripts
i = circumferential grid index
j = axial grid index

I. Introduction

The rotating detonation engine (RDE) is currently under investigation as an approach to achieving pressure gain combustion (PGC) for propulsion and power systems. The RDE essentially consists of an annulus with one end open (or having a throat and/or nozzle) and the other end valved (typically using non-mechanical, fluidic means). Fuel and oxidizer enter axially through the valved end. The detonation travels circumferentially. Combustion products exit predominantly axially through the open end. The majority of the fluid entering the device is passed over by the rotating detonation wave which, as a form of confined heat release, substantially raises the pressure and temperature. The fluid is then expanded and accelerated as it travels down the annulus. In principle, the flow exiting the device has a higher average total pressure than the flow that enters. The pressure gain of an RDE can be utilized to produce thrust directly, or it can be expanded through a turbine to produce additional useful work when compared to that from a conventional combustor which incurs a pressure loss when operating at the same inlet conditions and fuel flow rate.

The performance of RDE's is strongly affected by the inlet design. During the fill portion of the cycle, minimal restriction is sought between the supply manifold and the annulus. During the high pressure portion of the cycle (i.e. behind the detonation), the inlet is ideally closed. This prevents all backflow of hot gas into the supply manifold and also provides a thrust wall from which the post-detonative fluid can expand. Real-world RDE's typically have non-mechanical inlets that present a fixed restriction between the manifold and the annulus. The goal of their design is to minimize aerodynamic losses during inflow, and minimize backflow behind the rotating detonation. These are obviously competing objectives, and as such, real-world RDE inlet designs are a compromise between them.

Another factor that strongly affects RDE performance is the size of the throat that is provided at the exhaust end [1]. An exhaust throat reduces the fill Mach number, which in turn raises the pre-detonation pressure, and reduces inlet aerodynamic losses. As a result, performance can rise significantly when compared to the RDE with no exit throat. On its face, this result suggests that the exhaust throat should be as small as possible with the proviso that a reduced fill Mach number also implies the need for a physically larger device to accommodate the same amount of through-flow. However, RDE's complicate this suggestion. As will be shown, the presence of an exhaust throat gives rise to reflected waves that travel upstream to the inlet and affect the filling process. As such, there is more to consider with an RDE than average fill Mach number.

The Ref. [1] results exhibited an unexpected phenomenon that is related to the above complication and which is the major focus of the present work. Starting with an ideal inlet as described above (i.e. lossless to forward flow, closed to backflow) the Ref. [1] computational fluid dynamic (CFD) investigation found that with an exhaust restriction a mere 15% smaller than the RDE channel area, a major instability developed which grew in time to the point of causing detonation failure. The result was so unusual that it called into question whether it was a physical solution to the governing equations, or a manifestation of the numerical method used in the study. If it was the former, it would warrant further investigation into its mechanism of onset, and its sensitivities. Exploration of mitigation strategies would also be warranted since otherwise, a severe limitation would exist on the degree of exhaust throat

restriction allowed and by extension the maximum RDE performance possible. The present effort represents a preliminary step in the direction of such an investigation.

Basic CFD simulation descriptions, simplifying assumptions, and RDE configuration details will be provided first. The instability development and analysis will then be presented in detail using primarily the Ref. [1] simulation; hereinafter called the NASA code. It is then verified using an independently developed, and more highly resolved simulation[4]; hereinafter called the NRL code. Examination of output from the simulations will show that the instability has thermo-acoustic characteristics, but with a complex coupling pathway. Some relevant configuration and/or operational parameters are then examined in terms of their effect on the instability. These are the size of the inlet restriction, the inlet manifold pressure, the axial length, and the reactant equivalence ratio. It is shown that the RDE inlet restriction has the largest effect and that it is one of stabilization. An inlet restriction causes unavoidable aerodynamic loss. However, it is demonstrated that this loss is more than compensated for by the stabilizing effect, and that a high performance RDE configuration can be obtained.

II. Simulation Details

Both codes have been described in detail in the literature [1-4]. As such, only basic descriptions are provided here. They both assume that the RDE annulus has a high inner-to-outer diameter ratio allowing it to be 'unwrapped' and treated as a quasi-two-dimensional (Q2D) space (aka, channel). Within this channel, both codes solve the single-species, reactive Euler equations for a premixed, inviscid, adiabatic, calorically perfect gas using formally high-resolution schemes. The NASA code models only one gas, assumed to have properties that are an average of the reactants and products of combustion. The NRL code models two gases. Relevant parameter values for each code are shown in Table 1. The NASA code uses a very simple on-off, single constant finite rate reaction model. The NRL code uses an Arrhenius-type reaction rate model with an induction time sub-model to capture classical detonation features. The grid spacing of the NASA code is relatively coarse, while that of NRL is nearly an order of magnitude more refined (see Table 1). The rationales behind the code grid spacing choices are detailed in the literature [1-4].

Table 1 Dissimilar code parameters

Parameter	Value	
	NASA	**NRL**
Real gas constant, R_g (ft-lb$_f$/lb$_m$·R)	73.92	73.92-R/64.64-P
Ratio of specific heats, γ	1.264	1.403-R/1.243-P
Grid dimensions, cells	200 X 80	1413 X 565

Both codes impose boundary conditions which may be described as follows. Considering an RDE where the non-dimensional circumferential direction is x, and the axial direction is y, at x=0.0 and x=1.0, periodic (aka symmetric) conditions are used. These ensure that the x-dimension of the computational space faithfully represents an annulus (which is continuous and has no boundary). At $y=y_{max}$, constant ambient pressure outflow is imposed along with characteristic equations to obtain the density and axial velocity, ρ and v for the image cells. If the resulting flow is sonic, or supersonic, then the imposed pressure is disregarded. If, in addition, the upstream flow is supersonic, then p, ρ, and v are extrapolated from the interior. The possibility for a normal shock solution whereby supersonic outflow jumps to subsonic is also accommodated. The x-velocity component u is extrapolated from the interior at each boundary location. At y=0.0 (the inflow face), partially open boundary conditions are applied. This face is presumably fed by a large manifold at a fixed total pressure, and total temperature. The manifold terminates at the face and is separated from it via an orifice. The ratio of inlet orifice flow area to RDE annulus area, A_i/A_{ch}, is generally less than 1. If the interior pressure is less than the manifold pressure, P_m, then inflow occurs. The boundary condition routine determines p, ρ, and v for the inflow face image cells subject to a momentum (total pressure) loss model which depends on the mass flow rate and the value of A_i/A_{ch}. The routine is capable of accommodating a scenario where the inflow becomes choked. If A_i/A_{ch} is assigned a value of 1, a lossless inlet is ensured. The x-velocity component, u, is prescribed. Prescribing the negative of the detonation speed, u_{det}, yields solutions that are in the detonation frame of reference. Prescribing a value of zero yields solutions in the laboratory frame. If the interior pressure along the inlet face is greater than P_m, as might be found just behind the detonation, then the boundary condition routine implements a notional check-valve (i.e. a solid wall) which prevents backflow. In this work the detonation is traveling from right to left. As such, all computed u components in the detonation frame of reference are left to right.

Unless otherwise stated, both codes simulate a stoichiometric hydrogen/air mixture using the common parameters shown in Table 2, and channel area variation shown in Fig. 1. For clarity, the exit throat geometry may be described as a smooth, continuous area decrease over the last 15% of the axial length, which terminates with zero gradient.

Unless otherwise stated as well, all quantities are presented in non-dimensional form. The pressure, p, density, ρ, temperature, T, and velocity components, u and v are non-dimensionalized using dimensional reference states p^*=1.0 Atm., ρ^*=0.055 lb_m/ft^3, T^*=520 R, and the corresponding sound speed a^*=1250 ft/s, respectively. The distances, x and y are non-dimensionalized by the circumference, L. The time, t is non-dimensionalized using the reference wave transit time, L/a^*. The mixture specific heat of reaction is non-dimensionalized by the square of the reference speed of sound.

Table 2 Common code parameters

Parameter	Value
Manifold pressure, P_m, (Atm)	4.0
Manifold temperature, T_m, (R)	540
Ambient pressure, P_a, (Atm)	1.0
Axial length-to-circumference ratio	0.4
Stoichiometric fuel/air ratio	34.3
Fuel heating value, h_f, (BTU/lb_m)	51,571

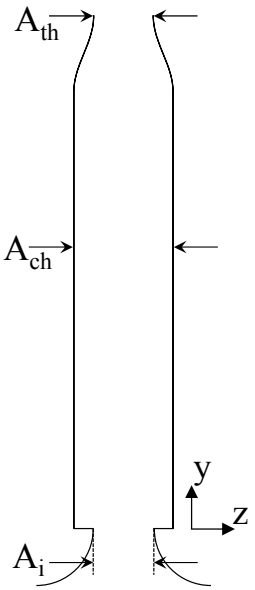

Fig. 1 RDE axial profile.

A. Performance Measurement

In this paper the performance metric of merit will be the ideal exhaust Equivalent Available Pressure (EAP_i) [5, 6]. EAP is essentially the pressure required to produce the specific thrust or work provided by the RDE, assuming that the flow is steady and homogeneous. It is thus a kind of average. EAP_i focuses on the RDE only to the point of the exit throat and disregards the expanding nozzle or whatever else exists downstream. It isolates the performance of the device itself, and is appropriate for numerical studies of the type provided here.

To compute the EAP_i, the exit plane of a converged RDE solution is examined and the following procedure is applied:

a) The ideal stream thrust for each numerical cell is computed. This is the thrust that would be produced if the fluid in the cell was isentropically expanded to ambient pressure.
b) The stream thrusts of all the numerical cells in the plane are summed to obtain a total flow ideal stream thrust.
c) This value is divided by the total mass flow rate to obtain an ideal specific thrust.
d) EAP_i is then obtained by computing the total pressure that provides the same total ideal specific thrust given a uniform flow at the mass flux-averaged exit total temperature of the RDE.

For reference, the mass flux-average of any quantity φ is defined as follows.

$$\overline{\varphi} = \frac{\sum_{i=1}^{N_x} \varphi_i \rho_i v_i}{\sum_{i=1}^{N_x} \rho_i v_i} \tag{1}$$

Here, the subscript i refers to each circumferential grid point in the exit plane (i.e. at the RDE throat).

III. Instability Development and Analysis

Consider an RDE operating with the Table 2 parameters, an ideal inlet (A_i/A_{ch}=1.0), and no exit throat (A_{th}/A_{ch}=1.0). The simulation is stable and, in the detonation frame of reference, the NASA code yields a solution which is invariant in time. When A_{th}/A_{ch} is reduced to 0.9, the pressure gain, EAP_i/P_m-*1*, increases from 50% to 63%. The solution remains stable and nearly steady. Reducing A_e/A_{ch} further from 0.9 to 0.85 initially results in an increase in pressure gain to 74%. Here, the word 'initially' means immediately after the weak shock wave caused by an instantaneous reduction in exit throat area has propagated upstream to the inlet and reduced the flow rate. In this case however, the solution does not remain stable. Figure 2 shows computed contours of temperature at successive times in the simulation beginning immediately after the initial transient just described. Initially, the contour plot looks as expected. The only notable feature is a reflection of the oblique wave from the exit contraction, upstream to the inlet. This occurs in any RDE configuration with an exhaust throat. As time progresses however, a certain 'waviness' or distortion begins to appear. The distortion is particularly evident in the fill boundary between post-detonation gas and incoming fresh charge (sometimes referred to as the deflagration zone since some reaction is actually occurring here).

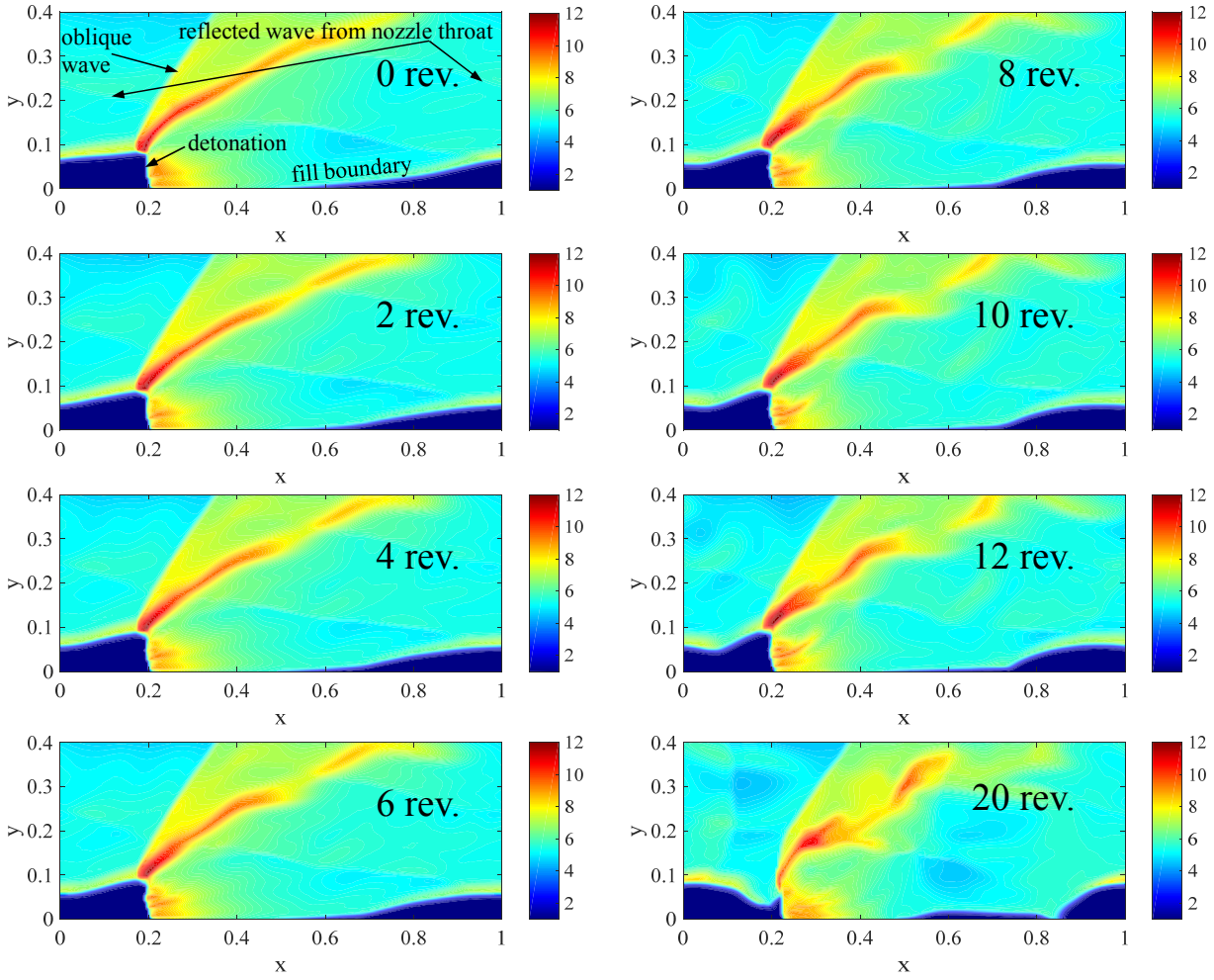

Fig. 2 NASA code computed contours of non-dimensional temperature at successive times in an idealized RDE with A_{th}/A_{ch}=0.85 and A_i/A_{ch}=1.0. The simulation is in the detonation frame of reference. Circumferential flow is left to right. Time is shown as the number of detonation revolutions.

The distortion continues to grow until it is profoundly affecting the flow field in general, and the detonation height in particular. Though not shown in Fig. 2, the distortion continues to grow in this simulation until the detonation eventually fails.

Figure 3 shows two temperature contours from a similar configuration to Fig. 2, but using the NRL code. Here, the instability onset occurred when A_e/A_{ch} was reduced from 0.95 to 0.9; a slightly higher ratio than that for the NASA code. This is likely due to the coarse grid of the NASA code which makes it more dissipative. Nevertheless, it is clear that the same instability is developing and growing in both simulations.

The duel observations that this instability requires the presence of internal shock reflections (propagating upstream toward the detonation front) in order to occur, and that contour plots such as those in Figs. 2 and 3 necessarily indicate large variations in the heat release rate, suggest that it is thermo-acoustic in nature. By this it is meant that a kind of in-phase coupling may be occurring between pressure fluctuations and heat release fluctuations. In order to test this notion, Rayleigh's criteria may be applied to the entire computing space (in the detonation frame of reference) and interrogated over time [7]. Rayleigh's criteria is a spatial integral which may be written in discrete form as follows.

$$R_c(t) = \sum_{i=1}^{N_x} \sum_{j=1}^{N_y} p'_{i,j} q'_{i,j} \Delta x \Delta y \tag{2}$$

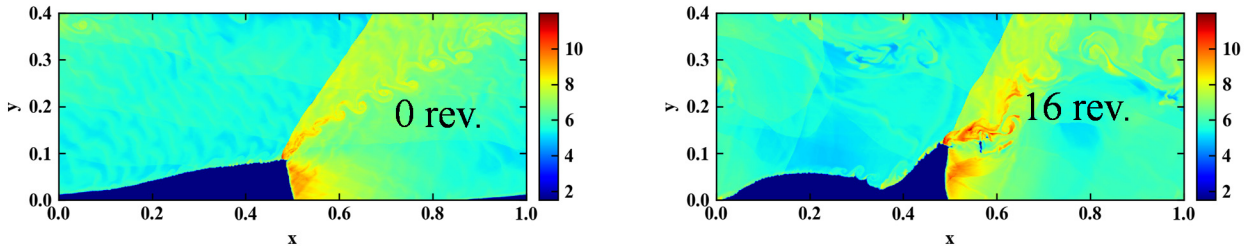

Fig. 3 NRL code computed contours of non-dimensional temperature at successive times in an idealized RDE with A_{th}/A_{ch}=0.90 and A_i/A_{ch}=1.0. The simulation is in the detonation frame of reference. Circumferential flow is left to right. Time is shown as the number of detonation revolutions.

Here, the subscripts i and j refer to the circumferential and axial grid indices. The fluctuating pressure and heat release rate quantities p' and q' are obtained at each point (i.e. each numerical cell) by first linearly fitting each p and q over a relatively long time period of interest (i.e. detrending [8]). For this work, a period of 4 wave revolutions will be used. Next, the linearly fitted p and q are subtracted from the instantaneous p and q at each discrete time step within the period ($p'=p-p_{detrend}$). If the time integral of R_c is positive and increasing over the interval, then the global pressure and heat release fluctuations are approximately in-phase and coupled, thereby adding destabilizing energy to the system. If R_c is periodic, it suggests that some sort of unstable cycle is developing. It is noted that positive R_c does not guarantee unstable behavior. Dissipative phenomena may be present which can either completely counteract the destabilizing forces, or limit them such that the instability does not grow indefinitely.

The Rayleigh criteria for the first four detonation revolutions of the NASA simulation in Fig. 2, are shown in Fig. 4. The time is scaled by the period for one detonation revolution around the annulus. Also shown in the figure are the spatial integrals of p' and q' alone (i.e. Eq. 2 with either p' and q' alone). It is evident that their time integrals are zero which indicates that the detrending operation described above was performed correctly. The actual Rayleigh integral, R_c is seen to be positive, cyclic, and growing in amplitude indicating that the instability is growing. It is interesting to contrast this clear indicator with the first 3 frames of Fig. 2 where the instability seems barely evident. Figure 5 shows the same integrals as Fig. 4 corresponding to the next four detonation revolutions of the Fig. 2 simulation (i.e. frames 3-5). Here the oscillations become more regular, and grow more rapidly (note the scale change between Figs. 4 and 5). Also shown in Fig. 5 is the Rayleigh criteria for the Fig. 3 NRL simulation. These results have been shifted in time by 6 detonation revolutions and thus correspond to revolutions 10 to 14. The overall trends of the two simulations are similar, including a regular instability period of 1/3 of a wave revolution. The rates of instability growth differ, but this is expected due to the facts that they are simulating slightly different configurations, and they differ in their grid resolution. The double peaked nature of the NASA code oscillations are evident in the last several oscillations of the NRL code. Regardless of the differences however, it is clear that both codes are simulating the same phenomena.

The exact mechanism by which the coupling demonstrated in Figs. 4 and 5 occurs is not completely understood at the time of this publication. There is partial understanding however, which may provide insight through its presentation.

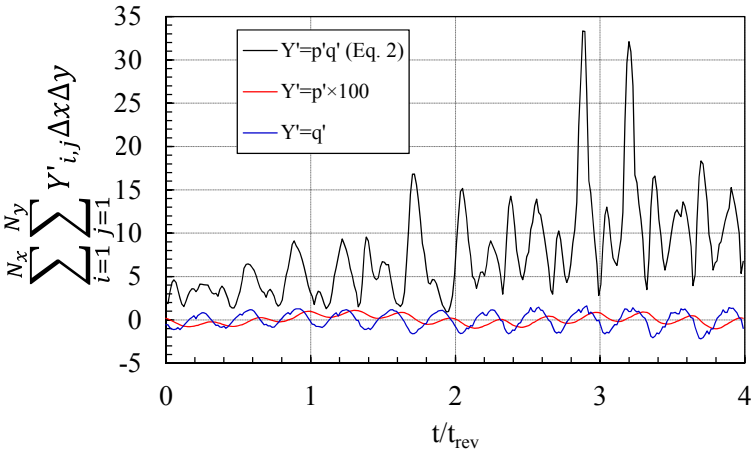

Fig. 4 Rayleigh criteria for the Fig. 2 NASA code simulation over the first four detonation revolutions.

Contour plots of the fluctuating quantities p', q', and $p'q'$ at t/t_{rev}=7.7 of Fig. 5 are shown in Fig. 6. The contour levels are truncated in order to highlight even small changes. It is evident from the central and lower contour plots that the vast majority of the energy input to the global Rayleigh criteria integral is occurring very locally, at the top of the detonation. It is also evident from the upper contour plot that no standing or resonant pressure wave pattern is developing, as would be evidenced by regular node and anti-node regions [7]. This is noted in order to point out that the instability, though clearly

satisfying Rayeigh's positive area criteria, is not classically thermo-acoustic. Finally, it is observed that the fill boundary is not monotonic. Instead it contains at least one 'ripple' which, in the detonation frame of reference is convected toward the detonation front.

These observations suggest the following informal pathway for the instability development. The reflected oblique wave propagates upstream until it interacts with the inflow and perturbs it. This perturbation (a momentary dip in the inflow velocity) is convected to the detonation and lowers the detonation height. The changing of the detonation height changes the position and strength of the oblique wave and its reflection. It also changes the circumferential position where fill inflow begins behind the detonation. These effects all serve to further distort the inflow, boundary and the subsequent detonation height; sometimes raising it, sometimes lowering it. A reexamination of Fig. 2 in light of this explanation clearly shows that the detonation height is varying with time.

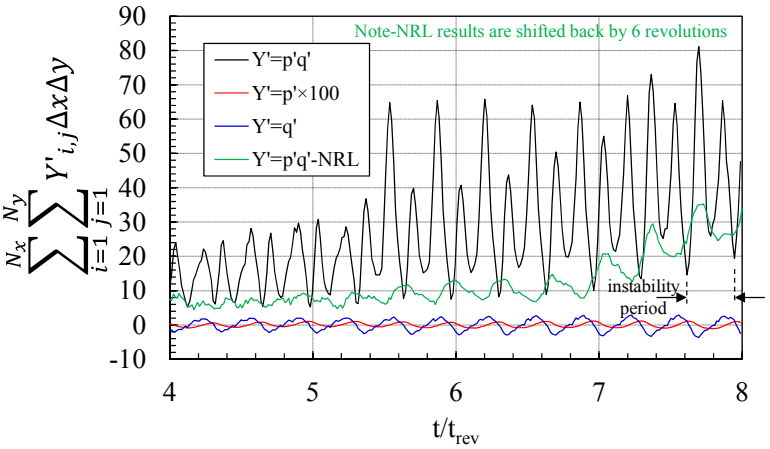

Fig. 5 Rayleigh criteria for the Fig. 2 NASA code simulation over the second four detonation revolutions. Also shown is the Rayleigh criterion for the Fig. 3 NRL code simulation.

That such a process is taking place is further evidenced by examining the mass flow rate information of Figs. 7 and 8. Figure 7 shows the mass flux in the inlet plane of the Fig. 2 simulation at t/t_{rev}=7.86. Two perturbations caused by reflected wave impingement are clearly evident in what is normally a smooth profile. Figure 8 shows average mass flow rate (across the entire inlet plane) during the same period as Fig. 5. The exit plane average mass flow rate is also shown. It is clear that the average inlet mass flow rate is oscillating, thereby implying an oscillation in the detonation height, and that the oscillation amplitude is growing.

This explanation for the instability pathway seems reasonable. However, it does not explain why the detonation height variation/inflow perturbation process is reinforcing, or why the particular period of the oscillations is observed. Furthermore, it cannot provide a predictive capability for when the throat area ratio will transition the flow field from stable to unstable. It is hoped that more insight will be gained at a later date. For the purposes of this paper, it is enough to reiterate that interactions between the inlet flow and the reflected waves are critical.

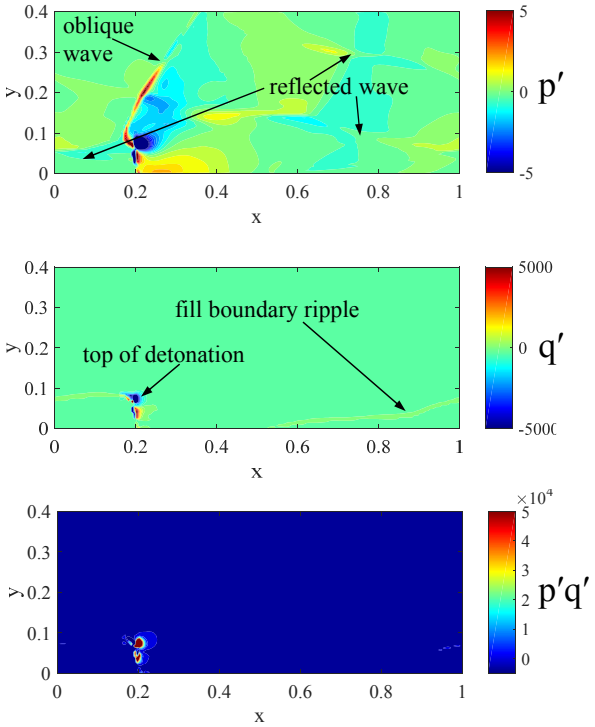

Fig. 6 Contour plots of the fluctuating quantities p', q', and $p'q'$ at t/t_{rev}=7.7 of Fig. 5.

IV. Instability Sensitivity

Given that the instability has now been demonstrated as a genuine one (albeit in an idealized environment), it is worthwhile to examine several relevant configuration or operational parameters to see which, if any, affect the instability onset. There are a number of such parameters to consider. In this work, the focus is on: the size of the inlet restriction, the axial length, the inlet manifold pressure, and the reactant equivalence ratio. All of the results provided in this section are from the NRL code. Select results have been verified with the NASA code to insure that trends are similar.

A. Inlet Restriction

Given the instability development pathway described in Section III, it is expected that introducing an inlet restriction would lead to stable operation at smaller values of A_{th}/A_{ch}. A simple restriction at the RDE inlet is a common laboratory approach to achieving non-mechanical valving (i.e. fluidically promoting forward flow, while minimizing backflow behind the detonation and providing a thrust surface). An inlet restriction makes the incoming flow less sensitive to perturbations from reflected waves because at least part of the inflow is choked, or nearly so. As such, it is likely to interfere with the instability development described earlier. Of course, the stabilization which may result from the inlet restriction cannot come without a cost. There is a sizeable aerodynamic loss associated with such a geometry (essentially a dump diffuser, or sudden expansion). The loss is modeled in both the NASA and NRL codes by boundary condition algorithms which impose a total pressure loss that increases as A_i/A_{ch}, decreases or as the mass flow rate increases. The algorithms are not the same for the two codes; however, they have been verified to produce the same levels of loss. Details of the loss models are not discussed here since the exact degree of inlet total pressure loss is less important in this simplified RDE simulation than the trends the loss reveals. More information on them can be found in Refs. [1-4]. As mentioned earlier, both codes also idealize the inlet restriction by preventing all backflow.

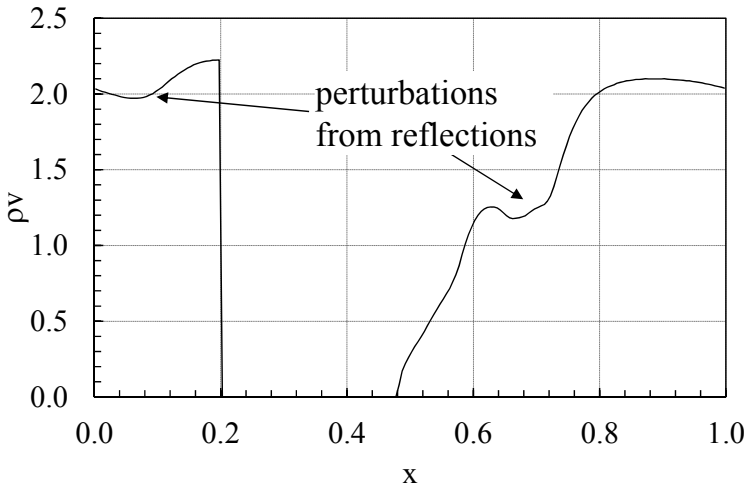

Fig. 7 Mass flux in the inlet plane of the Fig. 2 simulation at t/t_{rev}=7.86.

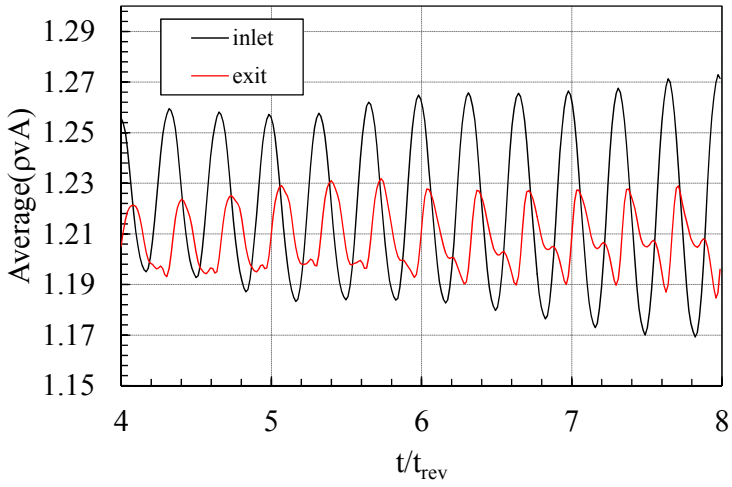

Fig. 8 Average mass flow rate (across the entire inlet plane) during the same period as Fig. 5.

Figure 9 summarizes the results of varying the inlet restriction. Here are shown curves of average EAP_i based pressure gain as functions of A_{th}/A_{ch}, for several families of A_i/A_{ch}. Also shown with each data point is the standard deviation. Both the average and the standard deviation are computed over the last 5 revolutions of a typically 20+ detonation wave revolution simulation. If the simulation is stable, the standard deviation is small (i.e. <5% on the scale shown). If the simulation is unstable, the standard deviation is large (i.e. >12%). It is noted that several of the simulation points yielded intermediate level standard deviation values. Interrogation of the flow field indicated that a kind of limit cycle is achieved where large fluctuations are occurring but not growing. These are still classified as unstable since they would not be considered practically reliable; at least until further investigation is conducted. An illustration of such a scenario is shown in Fig. 10. Contours of temperature are shown at two times after the limit cycle is established. The results were obtained with A_i/A_{ch}=0.6, and A_{th}/A_{ch}=0.55; a point which is not shown on Fig. 9 because it simply continued the downward trend shown. A clear wave-like pattern is evident, and the fill boundary is clearly distorted (or at least rippled). It appears that with the detonation height significantly reduced by the small exit throat, the possible variation in detonation height is limited as well. It is postulated that this gives rise to a limit cycle instead of a catastrophic instability.

The Fig. 9 results demonstrate that an inlet restriction does indeed stabilize the flow field, thereby allowing greater restrictions to be placed at the exit. They further demonstrate that for a particular combination of inlet and exit

restriction, the performance benefits from restricting the exit outweigh the aerodynamic losses imposed by the inlet. With the NRL code, this occurs when A_i/A_{ch}=0.6 and A_{th}/A_{ch}=0.7. At this point the RDE is indicating an impressive pressure gain of 62.1% which is nearly 6% above what can be achieved with a lossless inlet (A_i/A_{ch}=1.0) operating with acceptable stability (A_{th}/A_{ch}=0.95). This optimized performance is even more impressive when it is noted that the inlet loss model employed by the code predicts a 12% loss in total pressure due to the restriction. Here, the total pressure in the inlet plane is computed using an entropy averaging method described in Ref. [1]. Evidently, the stable detonation propagating through a low axial Mach number flow is more than compensating for the inlet loss in terms of producing useful pressure gain. Further exit restriction leads to unstable flow (and lower performance for this particular curve). Further inlet restriction leads to more stable flow, allowing for further exit restriction. However, inlet losses dominate and performance is reduced.

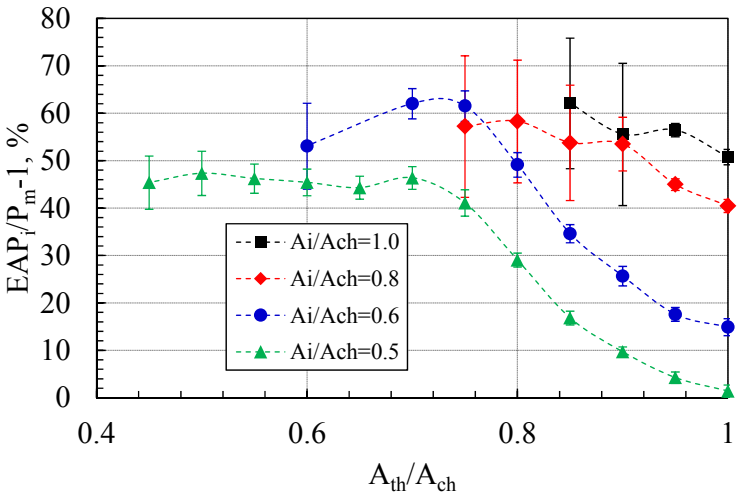

Fig. 9 EAP$_i$ pressure gain for the RDE described by Table 2 as a function of A_{th}/A_{ch} area for several families of A_i/A_{ch}.

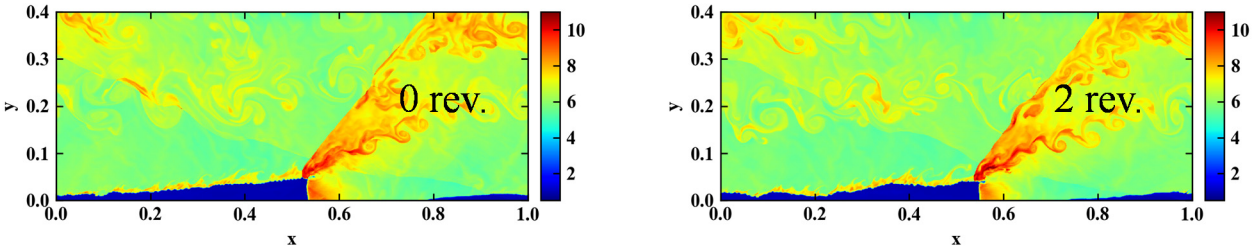

Fig. 10 Computed contours of non-dimensional temperature at two successive times during a limit cycle in an idealized RDE with A_{th}/A_{ch}=0.60 and A_i/A_{ch}=0.55. The simulation is in the detonation frame of reference. Circumferential flow is left to right. Time is shown as the number of detonation revolutions.

B. Axial Length

After analyzing the nature of the observed instability, the effect of the RDE axial length is hard to predict. On the one hand, there is no mechanism in the flow field to dissipate the reflected shock which appears to initiate the instability. Thus the only effect of changing the length would be to change where the reflection hit the inlet relative to the detonation position, and there is no indication that this position is consequential. On the other hand, it has already been noted that the phase relationship between inlet flow perturbation, detonation height variation, and instability reinforcement is not well understood. It does seem possible that axial length could have an impact here, yet the results shown in Fig. 11 suggest that it does not. Here the pressure gain of the RDE with the optimal inlet and exit restrictions from Fig. 9 is shown as a function of axial length. The standard deviation is unchanged by length, suggesting that stability is unaffected. The gradual improvement as the length is made shorter is likely the result of factors highlighted in Ref. [1]. The oblique wave and the high shear zone behind it (shown in Fig. 2) are both sources of entropy. The longer they are, the more entropy is generated, and the less ideal available pressure is produced at the exit. The cause of the large variation in pressure gain as the length gets shorter is unclear at this time.

C. Inlet Manifold Pressure

The instability is insensitive to changes in inlet manifold pressure as shown in Fig. 12. This is an expected result since, as indicated in Ref. [2], semi-idealized RDE CFD solutions such as those used here are largely invariant with manifold pressure once the exit flow is choked.

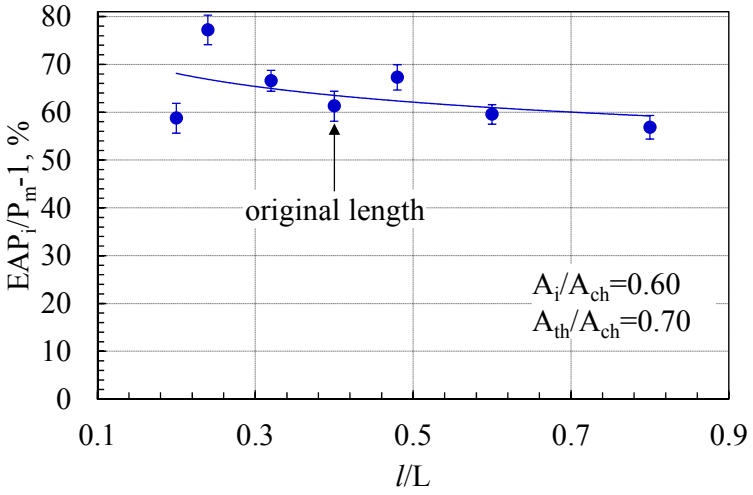

Fig. 11 EAP$_i$ pressure gain for the RDE described by Table 2 as a function of axial length.

D. Reactant Equivalence Ratio

Since the instability under investigation depends on heat release fluctuations, which in turn depend on the available chemical energy per unit of mass, it stands to reason that reducing the equivalence ratio, *ER*, may enhance stability. Of course, the pressure gain attainable in any pressure gain combustion process depends on the total chemical energy added [5]. As such, any stabilization observed with reduced *ER* must be considered in this light.

Figure 13 illustrates these expected trends. The plot shows EAP_i pressure gain as a function of A_{th}/A_{ch} for two values of A_i/A_{ch} and *ER*. For the case with A_i/A_{ch}=0.60, it is evident that the fluctuation levels are reduced (i.e. standard deviation is smaller), particularly at the lower values of A_i/A_{ch}. Unfortunately, this does not offer any benefit because the point at which instability is most reduced is already past the point of peak performance.

The results for A_i/A_{ch}=0.80 are quite different. Here the stability enhancement from the lower ER allows the exit throat to be reduced to A_{th}/A_{ch}=0.85 while still maintaining standard deviation levels below 5%. This is better performance than the best stable result attainable at the higher value of ER (A_i/A_{ch}>0.95). It implies increased pressure gain for less energy addition; an encouraging result.

V. Conclusion

An instability appearing in computational fluid dynamic (CFD) simulations of semi-idealized rotating detonation engines (RDE) configured with exit throats was described and verified. Verification was provided by demonstrating its existence in two independently developed CFD codes simulating the same configuration. The instability was shown to be thermo-acoustic in that pressure and heat release fluctuations are coupled and reinforcing. The exact mechanism of reinforcement is unclear, but appears to involve perturbations in the detonation height brought on by interactions between the inlet flow and waves that are reflected upstream from the exit throat. Its onset was shown to be closely linked to the sizes of the exit throat and the inlet restriction; both parameters that strongly influence RDE performance. Restricting the exit throat was shown to enhance performance, but promote instability growth. Restricting the inlet was shown to reduce performance, but provide stability. It was further shown that these competing effects can be optimized to yield a configuration with substantial pressure gain. Several other parametric sensitivities were also examined in terms of instability growth. It was found that axial length, and inlet manifold pressure had no effect. The equivalence ratio was shown to reduce instabilities as it was lowered. For some configurations, this was shown to allow for a smaller exit throat and thus enhanced stable performance. This study provided increased understanding of a largely unknown instability phenomenon that, while not yet observed in laboratory RDE's, may appear as their performance begins to approach these semi-idealized

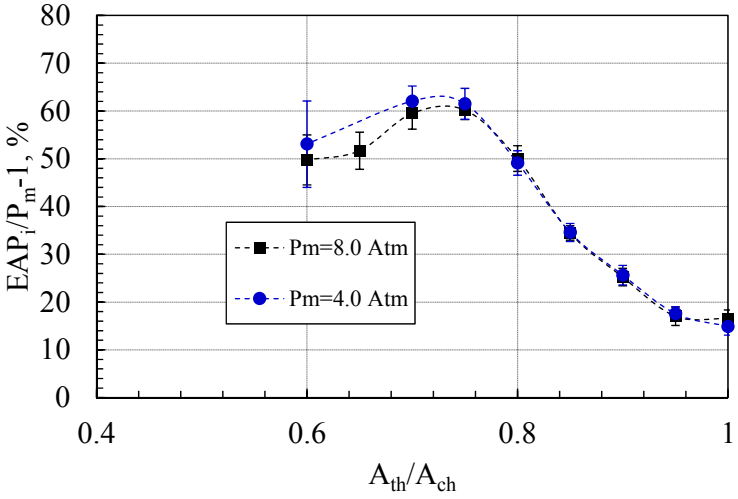

Fig. 12 EAP$_i$ pressure gain for the RDE described by Table 2 as a function of A$_{th}$/A$_{ch}$ area for two families of manifold pressure.

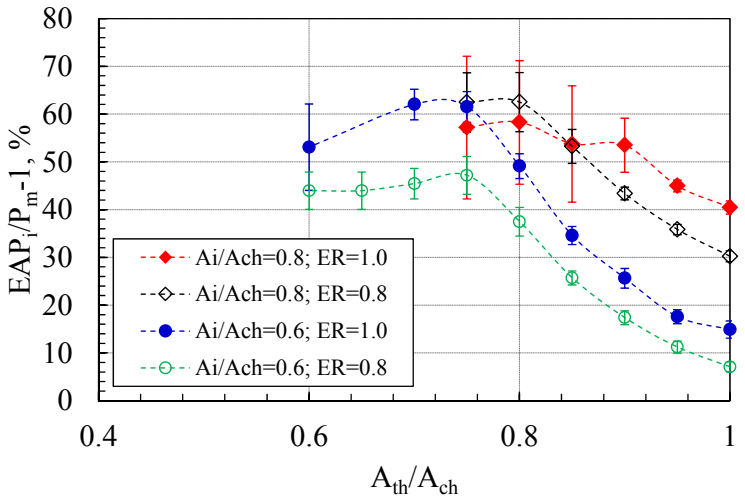

Fig. 13 EAP_i pressure gain for the RDE described by Table 2 as a function of A_{th}/A_{ch} area for two families of A_i/A_{ch} and ER.

simulations. It also provided thought-provoking input to the pressure gain combustion (PGC) community's ongoing discussion of realistic upper bounds on RDE performance.

References

[1] Paxson, D. E. "Impact of an Exhaust Throat on Semi-Idealized Rotating Detonation Engine Performance," AIAA-2016-1647, January, 2016, also NASA/TM-2016-219076.

[2] Paxson, D.E., "Numerical Analysis of a Rotating Detonation Engine in the Relative Reference Frame," AIAA-2014-0284, Jan., 2014, also NASA/TM 2014-216634, 2014.

[3] Paxson, D. E., Fotia, M. L., Hoke, J. L., Schauer, F. R., "Comparison of Numerically Simulated and Experimentally Measured Performance of a Rotating Detonation Engine," AIAA-2015-1101, Jan. 2015, also NASA/TM—2015-218835.

[4] Schwer, D. A., Kailasanath, K. "Numerical Investigation of Rotating Detonation Engines," AIAA-2010-6880, July, 2010.

[5] Paxson, D. E., Kaemming, T. A., "Foundational Performance Analyses of Pressure Gain Combustion Thermodynamic Benefits for Gas Turbines," AIAA 2012-0770, January 2012, also NASA/TM-2012-217443.

[6] Kaemming, T. A., Paxson, D. E., "Determining the Pressure Gain of Pressure Gain Combustion," AIAA-2018-4567, July, 2018.

[7] Nicoud F., Poinsot, T., "Thermoacoustic instabilities: Should the Rayleigh Criterion be Extended to Include Entropy Changes?" *Combustion and Flame*, V. 142, 2005, pp. 153-159.

[8] Kantz H., Schreiber T., Nonlinear Time Series Analysis, Cambridge University Press, 2004, p. 100.